# Analyzing the Electrical Performance of a Solar Cell with Time-Resolved Photoluminescence: Methodology for Fast Optical Screening

David M. Tex, Mitsuru Imaizumi, and Yoshihiko Kanemitsu

Phys. Rev. Applied **7**, 014019 — Published 26 January 2017

DOI: 10.1103/PhysRevApplied.7.014019

# Analyzing the electrical solar cell performance with time-resolved photoluminescence: Methodology of a fast optical screening technique

David M. Tex,[1] Mitsuru Imaizumi,[2] and Yoshihiko Kanemitsu[1,*]

[1] *Institute for Chemical Research, Kyoto University, Uji, Kyoto 611-0011, Japan*
[2] *Japan Aerospace Exploration Agency, Tsukuba, Ibaraki 305-8505, Japan*

The performance of solar cell devices is conventionally analyzed electrically by current–voltage measurements. To access the physics of the current generation process at the operating point, the analysis of fast optical responses from devices would be highly beneficial. However, the optical responses from pn-junctions exhibit a complex photoluminescence (PL) decay behavior due to their time-dependent electric fields. Here, we propose a method to systematically assign the physical meanings of the photoluminescence (PL) decay time constants by recording the complete excitation power dependence and voltage dependence of the time-resolved PL from a GaAs single junction. The experimentally obtained PL curves are in agreement with numerical predictions of dominant charge separation. We conclude that the charge separation can be directly observed in state-of-the-art devices. The experimental data set enables assignment of the effective separation time constant for the maximum output power condition, which is the most important number for understanding the carrier dynamics during device operation. The technique developed in this work constitutes a new characterization technique for solar cells.

## I. INTRODUCTION

The semiconductor solar cell technology exhibited a fast-paced growth over the last decades. Although the conversion efficiencies are approaching their predicted limits [1, 2], significant losses exist and optimization is still a key factor for large scale implementation of photovoltaics in future. For improving efficiencies, the carrier dynamics in the actual device have to be measured. The pn-junction is at the heart of the solar cell; it drives the current generation and has to be characterized carefully. Such a characterization can be performed electrically via current–voltage (I–V) curves, external quantum efficiency (EQE)[3, 4], electroluminescence (EL)[5–10] or also optically [11–13].

Characterization of optoelectronic devices with photoluminescence (PL) is fast, highly sensitive, contactless, and non-destructive. It is useful since PL directly reflects the device quality[14–17]. With regard to the information about the carrier dynamics, the PL spectra easily allow for individual characterization of different subcells, which is essential for tandem solar cell engineering. An important advantage over I–V techniques is that optical techniques can be applied before making electrical contacts. However, due to the inherent device properties, the optical responses are difficult to interpret [11]. Non-radiative recombination can be enhanced by point defects, while radiative recombination can be slowed down by carrier localization[18, 19]. Both effects are a result of extrinsic defects, but a even a high quality sample can exhibit fast and slow decay components due to intrinsic effects.

Several interpretations of PL decay dynamics from semiconcductor heterojunctions and also devices have been presented in the past and were based on numerical calculations [20, 21]. A highly interesting result is that in high-quality devices with band-to-band recombination, the charge separation [22, 23] of a device could be probed with an optical technique [21]. Unfortunately, only the very initial decay time constants were assigned to a physical property, and the complicated decay at high excitation powers and late times remained unassigned. A more intuitive and simplified interpretation of the PL decay curves for different excitation powers has been proposed recently, including experimental curves in excellent agreement with the theory [24, 25]. It was proposed that electrical performance can be evaluated without using any electrical contacts. However, the method based on analysis of time-resolved PL still requires a clear experimental foundation on a single junction to verify the model and assure reliable application.

The decay dynamics governed by Shockley-Read-Hall (SRH) recombination in a semiconductor layer can resemble those in pn-junctions [20, 21, 26]. Therefore, the usual interpretation of fast PL decays and a peculiar excitation power dependence in devices is the SRH recombination in either the n- or p-layer of the device, not related to the physics of a pn-junction diode. This is almost certainly true for devices containing materials with low luminescence yields or high number of interface defects [27]. However, in high-performance devices, the carrier transport plays a significant role in the PL decays. While simple power-dependence measurements are known to provide the trap-state properties in single layers of technically important materials [28–31], the known procedure is not able to distinguish between transport related and trap-state related PL decays in devices. A detailed investigation of the voltage dependence of PL decays from high quality pn-junctions is essential to clarify the physical meanings of the observed time constants.

In this work, we propose a fast and convenient optical method to characterize the electrical performance of so-

* kanemitu@scl.kyoto-u.ac.jp

lar cells. We investigate the excitation power dependence of time-resolved PL from a GaAs single junction under various bias conditions. When measuring the excitation power dependence of the device under open-circuit condition, three characteristic PL decay time constants are obtained in the low and high excitation power regime. The experimentally obtained curves are in very good agreement with numerical predictions in earlier works [21]. We find that the voltage dependence of the PL decays enables a clear assignment of the time constants. This experiment proves the physical meanings of the time constants. The most important time constant for device characterization is the effective separation time constant for the maximum output power condition. From our experiment we find that this time constant is almost identical with the PL time constant observed at late times and high excitation powers under open-circuit condition. Therefore we conclude that the charge separation can be directly observed in pn-junctions with the PL time constants obtained under high excitation power and open-circuit condition, which is highly useful for sample characterization since electrical contacts are not needed. The measurement of the time constants under high excitation power and open-circuit condition, combined with our proposed equation, constitutes a fast optical screening technique for solar cells.

## II. EXPERIMENTAL

The sample characterized in this work is a GaAs single-junction solar cell consisting of a top n-layer and a bottom p-layer. The thickness of the layers were 100 nm and 1500 nm for n- and p-layer, respectively. This solar cell has no anti-reflection coating and achieved a conversion efficiency of 18% with a fill factor $FF$ = 80%. For the time-resolved PL, we used a regenerative-amplifier Yb:KGW laser with an optical parametric amplifier (200kHz) for excitation with wavelength of 800 nm and a pulse width of about 200 ps. A streak camera with a monochromator and short- and longpass-filter sets were used for detection. All measurements were performed for a spot size with full-width at half maximum value of ≈150 $\mu$m. The detected PL was from the center of the excitation spot, with a full-width at half maximum value between 20 and 60 $\mu$m. The sample was measured in air and at room-temperature. The optical measurements were performed at open-circuit condition (power supply off) and for different forward-bias conditions ranging from 0 to 1.1 V using a direct-current voltage source and monitor equipment.

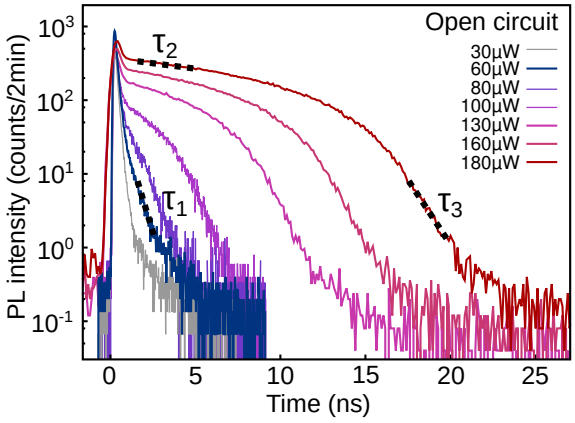


FIG. 1. Excitation power dependence of PL decay curves from the GaAs subcell showing fast response for low excitation and slow response for high excitation conditions.

## III. RESULTS

### A. Time-resolved photoluminescence

The excitation power dependence of the PL decay curves for open-circuit condition is shown in Fig. 1. All decay curves have an ultrafast initial response within the first nanosecond. Its time constant is faster than the measurement system's response time of 30 ps. For the lowest excitation power (30 $\mu$W), this initial ultrafast decay is dominant and followed by a weak multi-exponential decay. The intermediate time constant is about 500 ps, and the tail at late time has a time constant of about $\tau_{eq}$ = 1.5 ns (PL intensity level $I_{PL} \leq 1$). The PL intensity $I_{PL}$ is determined by the product of electron and hole densities. In the low PL intensity limit, $\tau_{eq}$ should reflect the minority carrier trapping time constant, which is a result of SRH recombination dynamics.

By increasing the excitation power to 60 $\mu$W, a fast decay time constant $\tau_1$ = 550 ps can be clearly observed at t=3 ns, which is between the initial ultrafast decay and $\tau_{eq}$. This intermediate PL contribution was also observed for lower excitation powers, but only when the excitation power is high enough, the long tail can be clearly observed. In the excitation power dependence from 60 to 160 $\mu$W, within the same time interval (Fig. 1, t=3 ns), we observe a drastic slow down of the decay time constant for higher excitation powers (factor 30). It reaches a value of $\tau_2$ = 15 ns for about 160 $\mu$W. By further increasing the excitation power, $\tau_2$ stays almost constant, which means that the slow time constant saturates for high excitation powers.

Immediately after excitation, the photocarrier density profile is determined by the exponential absorption with absorption coefficient $\alpha = 1.33 \times 10^4$/cm as shown in Fig. 2(a). For 30 $\mu$W, the volume average of the photocarrier density for a GaAs layer thickness of 1.6 $\mu$m would be $1.7 \times 10^{16}$ cm$^{-3}$. Under this condition the band pro-

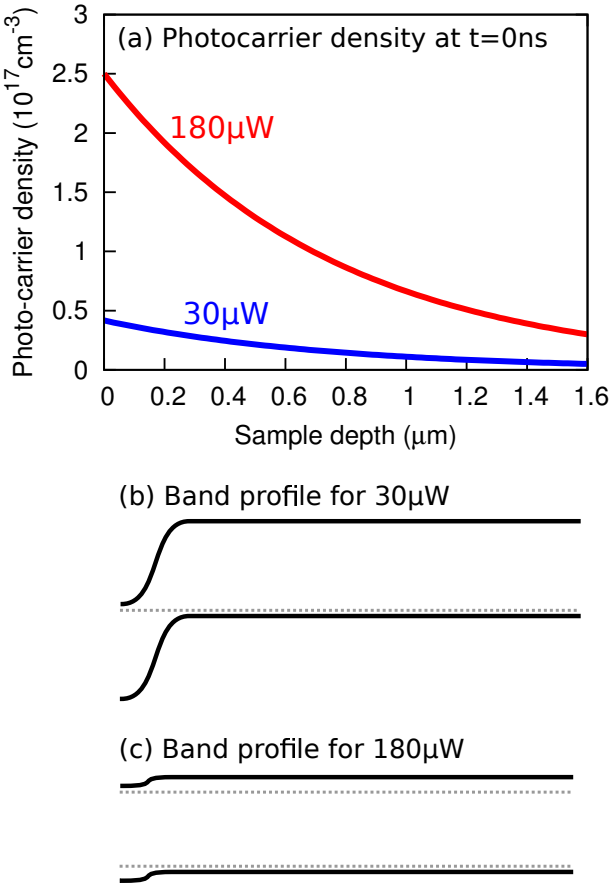


FIG. 2. (a) Initial photocarrier densities and (b) corresponding band structure after carrier diffusion for 30 and (c) 180 $\mu$W.

file stays almost in short-circuit condition (Fig. 2(b)). At 180 $\mu$W, the average photocarrier density is estimated to be about $1.04 \times 10^{17}$ cm$^{-3}$, which significantly exceeds the intended p-doping density of $1 \times 10^{16}$ cm$^{-3}$. Therefore the bands are expected to be almost flat after carrier diffusion (Fig. 2(c)).

We note that the dominant slow decay $\tau_2$ at high excitation powers is followed by a fast decay $\tau_3 = 1.2$ ns. The excitation power dependence of the fast time constant within the same PL intensity interval (Fig. 1, $I_{PL} = 3$) starting with $\tau_1$ shows a significant slow down (factor 3). After $\tau_3$, a further slow decay is observed (Fig. 1, $I_{PL} \leq 1$). This late PL decay occurs during quasi-equilibrium where drift current and carrier diffusion are balanced.

The above complicated excitation power dependence can be well explained if the PL dynamics at low carrier densities ($1 \leq I_{PL} \leq 10$) are determined by charge separation. Numerical simulations showed that in this case a minor change in the carrier densities can drastically alter the decay time constants $\tau_1$ and $\tau_2$ [21].

The general trend of the PL decays presented above has been also confirmed for other III-V materials [25]. Materials with lower mobility and larger number of defects are strongly influenced by these defects, and thus analysis of the transport properties becomes more difficult [27]. The excitation wavelength of 800 nm was chosen in order to excite the whole GaAs junction. By changing the wavelength to shorter regions, the surface volume will be excited, which introduces an additional decay component due to surface recombination. However, under high excitation conditions, this has only a small effect on the total PL decay, which has been confirmed for an InGaP subcell in a triple-junction solar cell [25].

### B. Time-resolved spectra

To clarify the origin of the observed PL, their spectra are shown in Figs. 3 (a) and (b). Figure 3 (a) is the time-resolved PL spectra for excitation with 80 $\mu$W under open-circuit condition. This slightly elevated excitation power was chosen since the two spectral and temporal regions can be distinguished easily. The broken line separates the time ranges where initial ultrafast decay and $\tau_1$ are observed. Both time regions show a clearly different PL spectrum. We observed the same behavior for the high excitation condition (160 $\mu$W), shown in Fig. 3 (b). The time region where $\tau_2$ is observed is blueshifted compared to the initial ultrafast response, and its spectral shape stays constant even for later times where $\tau_3$ is observed.

The time-integrated spectra are summarized in Fig. 3 (c). The PL during the decay $\tau_1$ is shown in green, and the contributions of $\tau_2$ and the EL signal obtained for 1 V bias are shown with the blue solid and broken curves, respectively. The PL peaks of $\tau_1$ and $\tau_2$ coincide with the EL peak, and these peaks appear at the band gap energy of GaAs $E_g = 1.42$ eV. The initial ultrafast decay (Fig. 3 (c); red data) has a peak at lower energies.

For high quality GaAs layers grown with molecular beam expitaxy, it has been reported that a dominant high energy peak from band-to-band transition is observed for n-doped samples, and a dominant low energy peak from the dopand-related transition for p-doped samples [33]. Therefore, we consider that the PL signals with peak around 870 nm are from the n-layer and the PL peak around 885 nm from the p-layer. Both $\tau_1$ and $\tau_2$ are a result of band-to-band recombination, while the ultrafast PL is related to the impurity PL, most likely from acceptors in the p-layer.

Although the p-layer is much thicker than the n-layer, the n-layer dominates the EL and $\tau_2$ signal. This means either a small luminescence efficiency of the p-layer or a strongly different Fermi-level splitting throughout the device. A strongly different Fermi-level splitting is possible in time regions where the system is far from equilibrium, which may the case for the first few tens of nanoseconds.

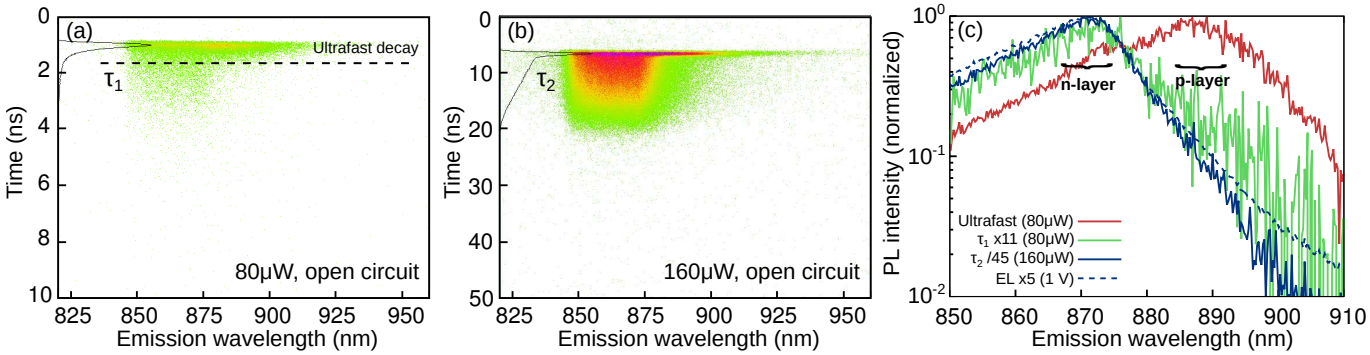


FIG. 3. (a) Time-resolved PL spectra of the sample for excitation with 80 $\mu$W, which corresponds to low excitation condition but with clear $\tau_1$ response. The two important temporal regions are separated with the broken line. (b) Time-resolved PL spectra of the sample for excitation with 160 $\mu$W, which corresponds to high excitation condition with clear $\tau_2$ response. (c) Time-integrated spectra of ultrafast time-regime (red solid line) and $\tau_1$ time regime (green solid line). In addition we also plotted the total time-integrated spectra observed for high excitation condition where $\tau_2$ is observed (blue solid line) and the EL signal for 1 V (blue broken line).

### C. Interpretation of time constants

Figure 1 showed a drastic slow down of the PL decay for increasing excitation power, which is analyzed in detail later in Fig. 5 (b). Given the saturation behavior of the time constant at high excitation conditions and expected low internal electric fields for an extended time range on the order of ten ns, we assign the dominant time constant $\tau_2$ to the intrinsic carrier recombination [24], *i.e.*, the long carrier lifetime in the bulk for carrier densities on the order of the doping level.

The time constant $\tau_1$ is assigned to the charge separation in the space-charge region [24]. The high electric field in this region for low carrier densities can effectively separate electrons and holes. If this separation process is faster than any trapping or recombination, which is the case for high mobility and/or low defect materials, the separation is directly reflected in the PL decay.

Under high excitation conditions, the carrier densities increase and thus $\tau_1$ becomes slower for higher excitation powers. This trend can be interpreted as follows. For high excitation powers, the initial fast carrier diffusion reduces the internal electric field and the pn-junction goes into flat-band condition. In this condition the bands are not necessarily flat, but the separation due to the electric field becomes a minor process, and the PL decay is determined by the carrier recombination time constant $\tau_2$. As the recombination proceeds, the pn-junction undergoes a transition from the flat-band (minor effect of electric field) to short-circuit condition (maximal internal electric field). Within this transition, there exists a time region in which the electric field contribution switches from minor to dominant. $\tau_3$ is assigned to the time constant which determines the carrier separation dynamics at the instant when the electric field becomes dominant again.

During light illumination, the carrier diffusion to the selective contacts is said to be the main driving force of the solar cell [32]. A pn-junction can work as selective contact. Close to the flat band condition, the electric field weakens and the mobility difference between electrons and holes becomes important. At the point of maximum output power under operation, the solar cell is in steady-state condition and current flows due to a difference between diffusion current and drift current components.

The time constant $\tau_3$ is observed slightly before the quasi-equilibrium PL begins to govern the PL decay, and therefore we consider that the drift current is still slightly larger than the diffusion current. This condition is almost identical with the operating point at the maximum output power of a solar cell [25]. However, this statement is only qualitative and requires a quantitative experimental verification, performed in the next section.
Another possibility to investigate the plausibility of the above assignments would be a theoretical analysis of the transient carrier dynamics in a pn-junction. Due to the complexity of the system, analytical solutions may be only derived using assumptions. Numerical simulations have been presented rarely in the literature [13], but the physical process behind the results are difficult to grasp. Therefore we consider that a simple yet elegant experiment is the most suited method to verify the meanings of the three time constants.

### D. Voltage dependence

To confirm the above physical interpretation of the time constants, we measure PL decay curves under different bias conditions. In Fig. 4 (a) the voltage dependence of the early time region for excitation with 60 $\mu$W is shown. The initial ultrafast decay did not change its intensity nor its time constant for any voltage. Therefore, the ultrafast initial response is assigned to the initial carrier separation by diffusion of the carrier density profile right after excitation. The maximum

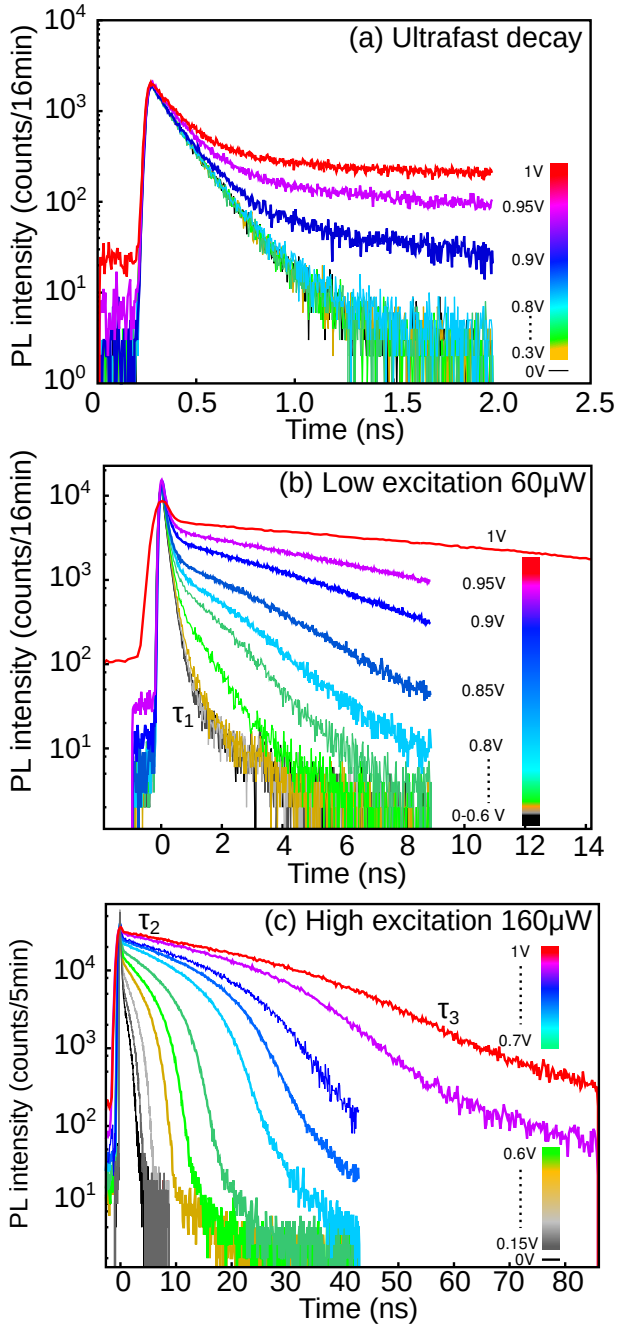


FIG. 4. Voltage dependence for (a) ultrafast regime under low excitation power of 60 $\mu$W, (b) short time regime under low excitation power of 60 $\mu$W, and (c) long time regime under high excitation power of 160 $\mu$W.

peak intensity showed no voltage dependence, since the initial carrier profile is not altered by the applied voltage. For high voltages of about 1 V the EL signal is observed as a background level, which is 100 times smaller than the PL peak signal and thus negligible.

Figure 4 (b) shows the bias voltage dependence for the low excitation power condition for a longer time range. This data is representative for the voltage dependence of the separation time constant $\tau_1$. Between 0 and 0.6 V the PL decay curves are similar to the that taken for open-circuit condition (Fig. 1, data for 60 $\mu$W), and show only a very small slow down. Between 0.7 and 1 V the PL decay time constant $\tau_1$ becomes drastically slower. We note that these PL decays can be fitted very well with a single exponential function and do not evolve into the the two exponential decay observed at high excitation powers (Fig. 1, data for 160 $\mu$W).

The slow down of $\tau_1$ and its single exponential behavior is considered to be a result of the reduction of the internal electric field due to external bias. Since the electric field is reduced, the charge separation proceeds slower. At a bias voltage of 1 V, $\tau_1$ reaches the saturated value of $\tau_2$ which was obtained for 160 $\mu$W excitation in the open-circuit condition.

The bias voltage dependence for the decay consisting of time constants $\tau_2$ and $\tau_3$ is shown in Fig. 4 (c). This data is measured for the excitation power 160 $\mu$W. The data for 0 V is much faster than the data for open-circuit condition (Fig. 1, data for 160 $\mu$W). This is considered to be a result of the forced charge separation due to the external bias. Conversely, by increasing the bias voltage, the decay approaches that for open-circuit condition and surpasses it in the high voltage regime (>0.7V). We find that both $\tau_2$ and $\tau_3$ are slowed down by the bias voltage. For 1 V bias, $\tau_3$ reaches the saturated value of $\tau_2$ which was obtained for 160 $\mu$W excitation in the open-circuit condition. On the other hand, at 1 V $\tau_2$ is already slower than the saturated value under open-circuit condition. We consider that a new emission mode alters the decay profile under high voltages, which induces an almost flat band over the whole sample area. The details are discussed in the next section.

Overall, the voltage dependence clarified that $\tau_1$ observed in the open-circuit condition is a time constant which corresponds to high electric fields, and $\tau_2$ as well as $\tau_3$ correspond to low electric fields. The experimentally observed bias dependence is consistent with our assignment of $\tau_1$, $\tau_2$, and $\tau_3$ given in the previous section and the explanation of dominant charge separation determined by the internal electric field.

## IV. DISCUSSION

The summary of the voltage dependence of the time constants is shown in Fig. 5 (a). The fast time constant $\tau_1$ obtained for excitation with 60 $\mu$W is shown with the open blue circles. From 0 V towards 0.7 V only a very small slow down is observed, but for higher voltages $\tau_1$ slows down drastically. This trend is roughly proportional to the inverse electric field in the space-charge region.

The voltage dependence of $\tau_3$ (Fig. 5 (a), blue filled circles), which was observed at late times for high excitation powers of 160 $\mu$W, is almost identical with that of

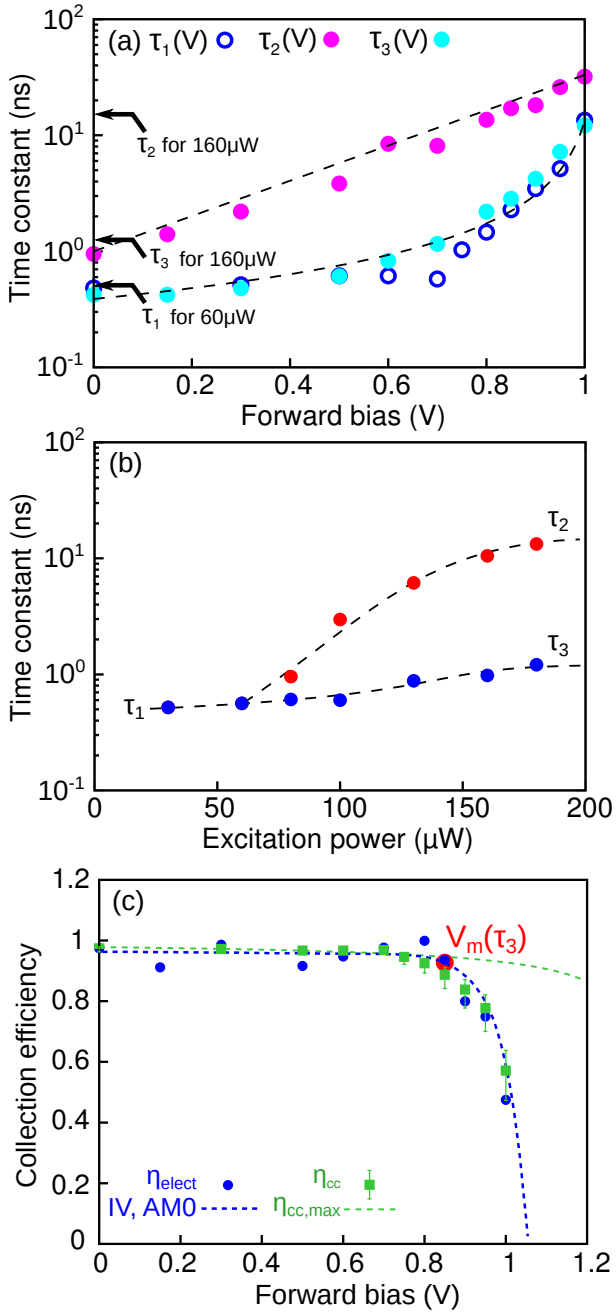


FIG. 5. (a) Summary of voltage dependence of time constants. The broken lines serve as an eye-guide. The three arrows indicate the saturated values which have been obtained in the open-circuit condition. (b) Excitation power dependence of time constants $\tau_2$ and $\tau_3$, beginning with 60 $\mu$W (the lowest power where both can be separated clearly for the first time). The broken lines serve as an eye-guide. (c) Comparison of collection efficiencies as determined by electrical and optical methods. The I–V curve obtained under AM0, 1 sun condition is plotted as well. The red dot ($V_m(\tau_3)$) indicates the operating voltage as determined from the crossing-point of $\eta_{cc}$ using $\tau_3$ and the I–V curve.

$\tau_1$. Independent of the excitation power, $\tau_1$ and $\tau_3$ are the same if the internal electric field is fixed by the external bias voltage. This strongly suggests that both time constants are determined by the internal electric field and constitute charge-separation time constants. Under open-circuit condition, $\tau_1$ is the charge-separation time constant corresponding to high electric fields which exist for low carrier densities, and $\tau_3$ is the charge-separation time constant corresponding to low electric fields which exist for high carrier densities.

The voltage dependence of the slow time constant $\tau_2$, obtained for high excitation powers, is shown with the purple filled circles in Fig. 5 (a). By increasing the voltage, $\tau_2$ becomes slower, without showing any indication for saturation. The gradual slow down is interpreted as improvement of photon recycling under high voltages and contribution of a non-decaying EL signal.

The excitation power dependence of the three time constants under open-circuit condition is shown in Fig. 5 (b). Above excitation power 60 $\mu$W, $\tau_1$ splits into $\tau_2$ (red filled circles) and $\tau_3$ (blue filled circles). The decay time constant $\tau_2$ quickly increases and approaches its saturated value of about 15 ns for 180 $\mu$W. This value corresponds to the $\tau_2$ measured for external bias of about 0.8 to 0.9 V. The time constant $\tau_3$ reaches about 1 ns for the high excitation condition, which is also obtained for external bias of about 0.7 to 0.8 V for both $\tau_1$ and $\tau_3$.

Figure 5 (c) compares the optically measured carrier collection efficiencies with the experimentally measured carrier collection efficiency and the I–V curves. The electrical carrier collection efficiencies can be determined directly from the experiment by measuring the photocurrent during pulsed excitation ($\Delta I_{pulse}$) and normalize by the absorbed number of photons ($\phi_{absorb}$),

$$\eta_{elect} = \frac{\Delta I_{pulse}}{q\phi_{absorb}} \ . \qquad (1)$$

The I–V curve of the device under AM0, 1 sun condition is also shown in this graph. Both, the electrical carrier collection efficiency (Fig. 5 (c), blue filled circles) and the I–V curve (Fig. 5 (c), blue broken curve) start to drop at 0.8 V. This indicates that the drop in the I–V curve, which determines the $FF$, is determined by the reduction of the carrier collection efficiency under high bias voltages.

The same trend can be also confirmed with the optical technique. The upper limit of the optically measured carrier collection efficiency is given by [24]

$$\eta_{cc,max} = \frac{1}{1+\frac{\tau_1}{\tau_2}\frac{1}{1-V/V_0}} \ , \qquad (2)$$

and shown with the green broken line. The time constants used in Eq. 2 are those obtained under open-circuit condition. To estimate the effect of the electric field, the charge separation time constant for maximum field ($\tau_1$) is scaled by the junction voltage $V$. The voltage is normalized by the gap voltage $V_0 = qE_g$, which means that this

curve is for an idealized high excitation condition. We confirm that up 0.8 V the upper limit agrees well with the electrical results, however, for higher voltages the values are strongly overestimated. This is because the upper limit cannot explain the dominant recombination by carrier diffusion, which occurs under low excitation densities ($V_{oc} < V_0$).

Since we measured the voltage dependence of the separation time constant directly, we can replace the scaling term $\frac{\tau_1}{1-V/V_0}$ directly with the measured value $\tau_1(V)$,

$$\eta_{cc} = \frac{1}{1 + \frac{\tau_1(V)}{\tau_2}} \ . \tag{3}$$

$\tau_2$ must be taken as a constant since it is the intrinsic recombination time constant. The result is shown with the green squares, including error bars. It is evident that this curve can explain the electrical carrier collection efficiency very well, supporting our physical interpretation of $\tau_1$.

Furthermore we can also evaluate the carrier collection efficiency at the point where the drift component starts to win over the carrier diffusion. This is done by replacing $\tau_1$ with $\tau_3$ obtained at open-circuit condition. We obtain $\eta = 1/(1 + 1.2/15) = 0.925$. By crossing the horizontal line $\eta = 0.925$ with the I–V curve we find a voltage of about 0.85 V (Fig. 5 (c), red point). This optically determined voltage is very close to the electrically determined voltage at maximum output power $V_m(IV) = 0.9$ V.

From the above we consider that the flat band condition is established for voltages above 0.9 V, and the junction voltage at which $\tau_3$ is observed should be around 0.85 V. This is close to the actual voltage at maximum output power $V_m(IV) = 0.9$ V at AM0, 1 sun. The good agreement strongly suggests that the operating point and $FF$ of a pn-junction is limited by the charge separation rate at high voltages ($\tau_3^{-1}$). Thus the optical method is able to predict the carrier collection efficiency close to the operating point of a pn-junction.

## V. CONCLUSION

In summary, we measured the excitation power dependence of time-resolved PL from a GaAs pn-junction under various bias conditions. Three characteristic time constants $\tau_1$, $\tau_2$, and $\tau_3$ were observed in the low and high excitation conditions. The PL spectral shape was analyzed to determine the origin of the time constants and we proposed a simple physical interpretation of the PL decays in pn-junctions. The unique behavior of the time-resolved PL intrinsic to pn-junctions was clarified and we stressed the importance of $\tau_3$ for solar cell characterization, which describes the carrier dynamics under device operation.

We consider that the present method can become a standard method for fast screening of wafer quality for solar cells, even before the wafer is processed and the solar cell's electrical contacts are actually deposited. This will be of high interest for solar cell researchers.

## ACKNOWLEDGMENTS

Part of this work was supported by JST-CREST.

[1] W. Shockley and H. J. Queisser, Detailed Balance Limit of Efficiency of p-n Junction Solar Cells, J. Appl. Phys. **32**, 510 (1961).

[2] M. Wolf, Limitations and Possibilities for Improvement of Photovoltaic Solar Energy Converters: Part I: Considerations for Earth's Surface Operation, Proc. IRE **48**, 1246 (1960).

[3] J. Burdick and T. Glatfelter, Spectral Response and I-V Measurements of Tandem Amorphous-Silicon Solar Cells, Solar Cells **18**, 301 (1986).

[4] M. Meusel, C. Baur, G. Letay, A. W. Bett, W. Warta, and E. Fernandez, Spectral response measurements of monolithic GaInP/Ga(In)As/Ge triple-junction solar cells: measurement artifacts and their explanation, Progr. Photovolt: Res. Appl. **11**, 499 (2003).

[5] U. Rau, Reciprocity relation between photovoltaic quantum efficiency and electroluminescent emission of solar cells, Phys. Rev. B **76**, 085303 (2007).

[6] T. Kirchartz, U. Rau, M. Hermle, A. W. Bett, A. Helbig, and J. H. Werner, Internal voltages in GaInP/GaInAs/Ge multijunction solar cells determined by electroluminescence measurements, Appl. Phys. Lett. **92**, 123502 (2008).

[7] S. Roensch, R. Hoheisel, F. Dimroth, and A.W. Bett, Subcell I-V characteristic analysis of GaInP/GaInAs/Ge solar cells using electroluminescence measurements, Appl. Phys. Lett. **98**, 251113 (2011).

[8] S. Chen, L. Zhu, M. Yoshita, T. Mochizuki, C. Kim, H. Akiyama, M. Imaizumi, and Y. Kanemitsu, Thorough subcells diagnosis in a multi-junction solar cell via absolute electroluminescence-efficiency measurements, Sci. Rep. **5**, 7836 (2014).

[9] L. Zhu, M. Yoshita, S. Chen, T. Nakamura, T. Mochizuki, C. Kim, M. Imaizumi, Y. Kanemitsu, and H. Akiyama, Characterizations of Radiation Damage in Multijunction Solar Cells Focused on Subcell Internal Luminescence Quantum Yields via Absolute Electroluminescence Measurements, IEEE J Photovolt. **6**, 777 (2016).

[10] R. Hoheisel, F. Dimroth, A. W. Bett, S. R. Messenger, P. P. Jenkins, and R. J. Walters, Electroluminescence analysis of irradiated GaInP/GaInAs/Ge space solar cells, Sol. Energy Mat. Sol. Cells **108**, 235 (2013).

[11] R. K. Ahrenkiel, B. M. Keyes, D. L. Levi, K. Emery, T. L. Chu, and S. S. Chu, Spatial uniformity of minority-carrier lifetime in polycrystalline CdTe solar cells, Appl. Phys. Lett. **64**, 2879 (1994).

[12] C. J. Bridge, P. Dawson, P.D. Buckle, and M.E. Özsan, Photoluminescence spectroscopy and decay time measurements of polycrystalline thin film CdTe/CdS solar cells, J. Appl. Phys. **88**, 6451 (2000).

[13] W. K. Metzger, D. Albin, D. Levi, P. Sheldon, X. Li, B. M. Keyes, and R. K. Ahrenkiel, Time-resolved photoluminescence studies of CdTe solar cells, J. Appl. Phys. **94**, 3549 (2003).

[14] O. D. Miller, E. Yablonovitch, and S. R. Kurtz, Strong Internal and External Luminescence as Solar Cells Approach the ShockleyQueisser Limit, IEEE J. Photovolt. **2**, 303 (2012).

[15] L. Zhu, T. Mochizuki, M. Yoshita, S. Chen, C. Kim, H. Akiyama, and Y. Kanemitsu, Conversion efficiency limits and bandgap designs for multi-junction solar cells with internal radiative efficiencies below unity, Opt. Express **24**, A740 (2016).

[16] Y. Yamada, T. Yamada, L. Q. Phuong, N. Maruyama, H. Nishimura, A. Wakamiya, Y. Murata, and Y. Kanemitsu, Dynamic Optical Properties of $CH_3NH_3PbI_3$ Single Crystals as Revealed by One- and Two-photon Excited Photoluminescence Measurements, J. Am. Chem. Soc. **137**, 10456 (2015).

[17] D. M. Tex, M. Imaizumi, H. Akiyama, and Y. Kanemitsu, Internal luminescence efficiencies in InGaP/GaAs/Ge triple-junction solar cells evaluated from photoluminescence through optical coupling between subcells, Sci. Rep. **6**, 38297 (2016).

[18] M. Baranowski, R. Kudrawiec, A. V. Luce, M. Latkowska, K. M. Yu, Y. J. Kuang, J. Misiewicz, C. W. Tu, and W. Walukiewicz, Influence of non-radiative recombination on photoluminescence decay time in GaInNAs quantum wells with Ga- and In-rich environments of nitrogen atoms , J. Appl. Phys. **111**, 063514 (2012).

[19] R. Kudrawiec, M. Syperek, M. Latkowska, J. Misiewicz, V.-M. Korpijärvi, P. Laukkanen, J. Pakarinen, M. Dumitrescu, M. Guina, and M. Pessa, Temperature evolution of carrier dynamics in $GaN_xPyAs_{1yx}$alloys, J. Appl. Phys. **117**, 175702 (2015).

[20] R. K. Ahrenkiel and M.S. Lundstrom, *Minority-carrier lifetime in III-V semiconductors: physics and applications*, Academic, 1993.

[21] W. K. Metzger, R. K. Ahrenkiel, J. Dashdorj, and D. J. Friedman, Analysis of charge separation dynamics in a semiconductor junction, Phys. Rev. B **71**, 035301 (2005).

[22] R. S. Crandall, Modeling of thin film solar cells: Uniform field approximation, J. Appl. Phys. **54**, 7176 (1983).

[23] S. Hegedus, D. Desai, and C. Thompson, Voltage dependent photocurrent collection in CdTe/CdS solar cells, Progr. Photovolt: Res. Appl. **15**, 587 (2007).

[24] D. M. Tex, T. Ihara, H. Akiyama, M. Imaizumi, and Y. Kanemitsu, Time-resolved photoluminescence measurements for determining voltage-dependent charge-separation efficiencies of subcells in triple-junction solar cells, Appl. Phys. Lett. **106**, 013905 (2015).

[25] D. M. Tex, M. Imaizumi, and Y. Kanemitsu, Charge separation in subcells of triple-junction solar cells revealed by time-resolved photoluminescence spectroscopy, Opt. Express **23**, A1687 (2015).

[26] N.H. Karam, R.R. King, B.T. Cavicchi, D.D. Krut, J.H. Ermer, M. Haddad, L. Cai, D.E. Joslin, M. Takahashi, J.W. Eldredge, W.T. Nishikawa, D.R. Lillington, B.M. Keyes, and R.K. Ahrenkiel, Development and Characterization of High-Efficiency $Ga_{0.5}In_{0.5}P$/GaAs/Ge Dual- and Triple-Junction Solar Cells, IEEE Trans. Electron Dev. **46**, 2116 (1999).

[27] Y. Yamada, T. Yamada, A. Shimazaki, A. Wakamiya, and Y. Kanemitsu, Interfacial Charge-Carrier Trapping in $CH_3NH_3PbI_3$-Based Heterolayered Structures Revealed by Time-Resolved Photoluminescence Spectroscopy, J. Phys. Chem. Lett. **7**, 1972 (2016).

[28] H. Yasuda and Y. Kanemitsu, Dynamics of nonlinear blue photoluminescence and Auger recombination in $SrTiO_3$, Phys. Rev. B **77**, 193202 (2008).

[29] H. Yasuda, Y. Yamada, T. Tayagaki, and Y. Kanemitsu, Spatial distribution of carriers in $SrTiO_3$ revealed by photoluminescence dynamics measurements, Phys. Rev. B **78**, 233202 (2008).

[30] C. R. Haughn, K. J. Schmieder, J. M. O. Zide, A. Barnett, C. Ebert, R. Opila, and M. F. Doty, Quantification of trap state densities in GaAs heterostructures grown at varying rates using intensity-dependent time resolved photoluminescence, Appl. Phys. Lett. **102**, 182108 (2013).

[31] Y. Yamada, T. Nakamura, M. Endo, A. Wakamiya, and Y. Kanemitsu, Photocarrier Recombination Dynamics in Perovskite $CH_3NH_3PbI_3$ for Solar Cell Applications, J. Am. Chem. Soc. **136**, 11610 (2014).

[32] P. Würfel, *Physics of Solar Cells: from Basic Principles to Advanced Concepts*, New York, USA, Wiley 2009.

[33] G. Borghs, K. Bhattacharyya, K. Deneffe, P. Van Mieghem, and R. Mertens, Band-gap narrowing in highly doped n- and p-type GaAs studied by photoluminescence spectroscopy, J. Appl. Phys. **66**, 4381 (1989).